HHS Public Access

Author manuscript

*Int J Cardiol*. Author manuscript; available in PMC 2016 November 07.

Published in final edited form as:

*Int J Cardiol*. 2014 January 1; 170(3): 426–433. doi:10.1016/j.ijcard.2013.11.034.

# Blood flow characteristics in the ascending aorta after aortic valve replacement—a pilot study using 4D-flow MRI☆,,☆☆

**Florian von Knobelsdorff-Brenkenhoff**[a,*], **Ralf F. Trauzeddel**[a], **Alex J. Barker**[b], **Henriette Gruettner**[a], **Michael Markl**[b,c], and **Jeanette Schulz-Menger**[a]

[a]Working Group on Cardiovascular Magnetic Resonance, Experimental and Clinical Research Center, a joint cooperation between the Charité Medical Faculty and the Max-Delbrueck Center for Molecular Medicine; and HELIOS Klinikum Berlin Buch, Department of Cardiology and Nephrology, Berlin, Germany

[b]Department of Radiology, Feinberg School of Medicine, Northwestern University, Chicago, IL, USA

[c]Department of Biomedical Engineering, McCormick School of Engineering, Northwestern University, Chicago, IL, USA

## Abstract

**Background—**Aortic remodeling after aortic valve replacement (AVR) might be influenced by the postoperative blood flow pattern in the ascending aorta. This pilot study used flow-sensitive four-dimensional magnetic resonance imaging (4D-flow) to describe ascending aortic flow characteristics after various types of AVR.

**Methods—**4D-flow was acquired in 38 AVR patients ($n = 9$ mechanical, $n = 8$ stentless bioprosthesis, $n = 14$ stented bioprosthesis, $n = 7$ autograft) and 9 healthy controls. Analysis included grading of vortex and helix flow (0–3 point scale), assessment of systolic flow eccentricity (1–3 point scale), and quantification of the segmental distribution of peak systolic wall shear stress ($WSS_{peak}$) in the ascending aorta.

**Results—**Compared to controls, mechanical prostheses showed the most distinct vorticity (2.7 ± 0.5 vs. 0.7 ± 0.7; $p < 0.001$), while stented bioprostheses exhibited most distinct helicity (2.6 ± 0.7 vs. 1.6 ± 0.5; $p = 0.002$). Instead of a physiologic central flow, all stented, stentless and mechanical prostheses showed eccentric flow jets mainly directed towards the right-anterior aortic wall. Stented and stentless prostheses showed an asymmetric distribution of $WSS_{peak}$ along the aortic circumference, with significantly increased local $WSS_{peak}$ where the flow jet impinged on the aortic wall. Local $WSS_{peak}$ was higher in stented (1.4 ± 0.7 $N/m^2$) and stentless (1.3 ± 0.7 $N/m^2$) compared to autografts (0.6 ± 0.2 $N/m^2$; $p = 0.005$ and $p = 0.008$) and controls (0.7 ± 0.1

---

☆All authors take responsibility for all aspects of the reliability and freedom from bias of the data presented and their discussed interpretation.

☆☆Acknowledgement of grant support: FvKB is supported by the Else Kröner-Fresenius Stiftung (Bad Homburg, Germany). AJB is funded by the Whitaker Postdoctoral and Fulbright Grants (New York, USA). MM is supported by the NMH Excellence in Academic Medicine (EAM) Program ‘Advanced Cardiovascular MRI Research Center’ (Chicago, USA).

*Corresponding author at: Working Group on Cardiovascular Magnetic Resonance; Charité Medical Faculty Berlin, Experimental and Clinical Research Center, Lindenberger Weg 80, 13125 Berlin, Germany. Tel.: +49 30 450 540 654; fax: +49 30 450 540915. florian.von-knobelsdorff@charite.de (F. von Knobelsdorff-Brenkenhoff).

N/m$^2$; $p = 0.017$ and $p = 0.027$). Autografts exhibited lower absolute $WSS_{peak}$ than controls (0.4 ± 0.1 N/m$^2$ vs. 0.7 ± 0.2 N/m$^2$; $p = 0.003$).

**Conclusions—**Flow characteristics in the ascending aorta after AVR are different from native aortic valves and differ between various types of AVR.

### Keywords

Aorta; Hemodynamics; Magnetic resonance imaging; Surgery; Valves; 4D-flow

## 1. Introduction

After aortic valve replacement (AVR), thoracic aortic remodeling is observed, which includes progression, stagnation or regression of aortic dilatation and mainly occurs in the aortic root and mid-ascending aorta [1,2]. The mechanism of interaction between AVR and ascending aortic remodeling is unknown, yet certainly multifactorial. The known parameters related to this process include genetic predisposition, aortic wall morphology, atherosclerotic risk profile, as well as nature of the original valvular lesion [3]. In addition, ascending aortic hemodynamics after AVR and their possible connection to aortic remodeling are of interest. Post-stenotic regions or asymmetries in the local geometry create a highly dynamic flow environment where wall shear stress (WSS) is characterized by abrupt changes in magnitude and direction during the cardiac cycle. A non-uniform distribution of wall shear stress with abnormally high levels at the flow impingement site is the driving force behind wall degradation and predispose to aneurysm formation and growth. Low levels are associated with inflammation and endothelial cell dysfunction and promote atherosclerotic changes [4,5].

Local flow measurements and flow visualizations are possible with time-resolved three-dimensional flow-sensitive cardiovascular magnetic resonance (4D-flow CMR). Helicity and vorticity can be visualized, and the distribution of aortic WSS can be estimated [6–8]. The feasibility of 4D-flow adjacent to various aortic heart valve prostheses has been demonstrated in a flow phantom [9]. In the present pilot study, 4D-flow was applied in patients after various types of AVR and in healthy controls to describe the ascending aortic flow characteristics after AVR in order to generate hypotheses for future research in larger samples.

## 2. Methods

### 2.1. Study sample

The local ethics committee approved the study and written informed consent was obtained from the individuals. Fifty consecutive patients with surgical AVR and 9 healthy controls were prospectively enrolled. The types of AVR included mechanical prostheses, stented and stentless bioprostheses, as well as autografts (Ross procedure: replacement of the native aortic root by the pulmonary root). Transapically/transfemorally implanted prostheses were not included. Mechanical and stented prostheses were implanted in the supra-annular position. Twelve patients were excluded: in 8, extensive respiratory motion hindered efficient navigator control, 2 presented with atrial fibrillation, 1 interrupted the exam due to

claustrophobia and 1 did not fit into the scanner due to obesity. The status “healthy” of the controls was based on: i) uneventful medical history, ii) absence of any symptoms indicating cardiovascular dysfunction, and iii) normal cardiac dimensions and function, normal morphology and function of the aortic valve and normal sized thoracic aorta on CMR cine imaging. In total, 38 patients with surgical AVR and 9 controls comprised the final study sample. Their characteristics are summarized in Table 1.

### 2.2. Image acquisition protocol

All subjects underwent CMR at a 1.5 T MR system (Avanto, Siemens Healthcare, Erlangen, Germany). Image acquisition settings and protocols were identical in all participants. A 12-channel body array coil was used for reception and the body coil for transmission. No contrast agent was administered.

Time-resolved 3D phase contrast CMR with three-directional velocity encoding (4D-flow) was acquired in a sagittal oblique volume covering the thoracic aorta using prospective ECG gating and a respiratory navigator placed on the lung–liver interface [6]. The phase contrast data were acquired with a Cartesian sampling pattern. Typical scan parameters were: echo time [TE] = 2.3 ms, repetition time [TR] = 4.8 ms, bandwidth = 440 -Hz/pixel, acceleration mode GRAPPA with factor 2 and 24 reference lines, flip angle $\alpha$ = 9°, temporal resolution 38.4 ms, field of view [FOV] 400 × 375 mm, matrix 192 × 158, voxel size 2.1 × 2.4 × 2.2 $mm^3$, 1 slab, phase encoding direction a-p, number of slices 26, slice thickness 2.2 mm, and slab thickness 57.2 mm. Velocity encoding was set to 2.5 m/s based on empirical data of the peak velocity in the ascending aorta after AVR to provide appropriate signal-to-noise at least during systole while omitting significant aliasing. The navigator acceptance window was set to 14 mm, navigator search window 48 mm. Image acquisition was interrupted if less than 50% of the image data could be acquired within 15 min of scanning. Another attempt was started after repeated breathing instructions and loading the abdomen with a sand bag. If again, less than 50% of the image data could be acquired within 15 min of scanning, the subject was excluded from enrollment. Efficient navigator control was assumed if > 50% of data were acquired within less than 15 min. Mean scan duration was approximately 20 min.

To assess left ventricular function and dimensions as well as the orifice area of the AVR, ECG-gated, breath-held steady-state free-precession (SSFP) cine imaging was performed as previously reported [10]. Aortic size was estimated from axial SSFP imaging of the thorax [11].

### 2.3. Image processing and analysis

Image processing was performed as described previously and included noise filtering, eddy-current correction, and velocity aliasing correction (MatLab; The MathWorks, Natick, MA, USA) [6]. A 3D phase contrast MR angiogram was calculated and used for flow visualization (EnSight, CEI, Apex, NC). Three analysis planes were positioned perpendicular to the aortic wall at the level of the sinotubular junction (S1), the mid-ascending aorta (at the level of the pulmonary bifurcation) (S2), and proximal to the brachiocephalic trunk (S3) (Fig. 1) [6]. These locations were chosen to be in concordance with recommended aortic measurement levels [12], and to keep appropriate distance to the

prosthetic level to omit the influence of susceptibility artifacts. The time-resolved data from these planes were exported to an analysis tool, segmented and used for WSS quantification (Flow tool; MatLab; The MathWorks, Natick, MA, USA) [13]. Image analysis focused on the systolic flow phase to omit errors attributed to measurement noise, which may be relevant in diastolic flow that is slow in relation to the VENC setting. The procedural stability of this technique has been shown in a number of studies reporting acceptable inter- and intra-observer WSS variability and scan–rescan reproducibility [7,13,14].

Left ventricular chamber quantification and prosthetic orifice area planimetry were done by manual segmentation using commercial software (CMR42, Circle Cardiovascular Imaging, Calgary, Canada) [10]. The orifice areas of the mechanical prostheses were taken from published reference values, as MR-planimetry is not feasible due to artifacts [15]. Aortic size was estimated on the level of the midpoint between sinotubular junction and the origin of the innominate artery.

### 2.4. Evaluation of blood flow vortex and helix in the ascending aorta

Flow vortex and helix were evaluated in the ascending aorta using particle traces and systolic streamlines in a complementary approach by consensus of two readers. Streamlines represent the instantaneous path tangent to the velocity vectors at a specific point in time. Particle traces display the temporal evolution of the blood flow velocity data over one heartbeat. Semi-quantitative visual analysis focused on the presence and extent of helix and vortex flow particularly during systolic and early diastolic flow. Vortex flow was defined as revolving particles around a point within the vessel with a rotation direction deviating by more than 90° from the physiological flow directions within one heartbeat. Helix flow was considered regional fluid circulation around an axis parallel to bulk fluid motion (i.e. along the longitudinal axis of the vessel), thereby creating a corkscrew-like motion. Helix and vortex strengths were graded in 4 categories: 0 = none, 1 = mild (flow rotation b360°), 2 = moderate (flow rotation N360°), 3 = severe (flow-rotation ≫360°) [16].

### 2.5. Evaluation of blood flow eccentricity in the ascending aorta

Two-dimensional velocity maps of analysis plane S2 were evaluated by consensus of two readers regarding the eccentricity of the ascending aortic flow in systole as described in the literature [7] (Fig. 1): 1 = normal flow if high velocity systolic flow was centrally focused, occupying the majority of the vessel lumen. 2 = mild eccentric flow if high velocity systolic flow occupied between one- and two-thirds of the vessel lumen. 3 = marked eccentric flow if high velocity systolic flow occupied one-third or less of the vessel lumen.

### 2.6. Quantification of wall shear stress in the ascending aorta

Peak WSS ($WSS_{peak}$; unit $N/m^2$) in the ascending aorta was calculated based on time-resolved flow data [13]. $WSS_{peak}$ corresponds to the peak value during systole at a single time frame. Quantification was performed for 12 segments along the aortic circumference (Fig. 1) for each analysis plane S1–S3 to analyze local variations [6].

### 2.7. Statistical methods

Continuous data are expressed as mean ± standard deviation (SD) and categorical data are expressed as frequency or percentage. Groups were compared using the Kruskal–Wallis test. In case of a significant test result individual group-to-group comparisons were performed by a Mann–Whitney-*U* test. Statistical significance was set at a probability level of b0.05. Analysis was performed using SPSS Statistics 20.0 (IBM, Armonk, US).

## 3. Results

### 3.1. Patients' demographics and cardiovascular information

The results for patients' demographics and cardiovascular dimensions are summarized in Table 1. Patients with stented bioprostheses were significantly older than those with mechanical prostheses and autografts as well as controls (each $p < 0.001$). The latency since valve implantation was shorter for stentless ($p = 0.015$) and stented bioprostheses ($p = 0.003$) compared to mechanical valves. Labeled valve size was significantly larger in stentless compared to stented bioprostheses ($p = 0.007$). Both orifice area and orifice area indexed by body surface area were larger in autograft recipients and controls compared to stentless ($p < 0.001$; $p = 0.001$), stented (each $p < 0.001$) and mechanical prostheses (each $p < 0.001$). Moreover, stentless prostheses exhibited larger orifice areas than stented devices ($p = 0.010$). The ascending aorta was larger in patients with stented ($p = 0.001$), mechanical ($p = 0.001$) and autografts ($p = 0.016$) compared to controls. Three out of the 7 patients with autografts had bicuspid aortic valve disease. The mechanical group had a lower ejection fraction compared to controls ($p = 0.004$). There were no intergroup-differences regarding left ventricular end diastolic volume ($p = 0.459$), stroke volume ($p = 0585$) and interventricular septum thickness ($p = 0.066$).

### 3.2. Blood flow pattern in the ascending aorta: vorticity, helicity and eccentricity

Blood flow visualization and interpretation were feasible in all subjects. As susceptibility artifacts were expectedly present in mechanical prostheses and stented bioprostheses, the prosthetic level was not included in the assessment. Fig. 2 summarizes flow visualizations for each AVR type and Fig. 3 exemplarily illustrates the differences in flow patterns present in a control subject and two AVR subjects with severe vorticity and helicity. Fig. 4 provides a synopsis of the scoring of blood flow vorticity, helicity and eccentricity.

Mechanical prostheses received the largest vorticity scores, which differed significantly from stentless bioprostheses ($p = 0.020$), autografts ($p = 0.007$) and controls ($p < 0.001$). Stented bioprostheses exhibited the second highest vorticity scores, which also differed significantly from stentless bioprostheses ($p = 0.036$), autografts ($p = 0.011$) and controls ($p < 0.001$). Stented bioprostheses received higher helicity scores than stentless bioprostheses ($p = 0.048$), autografts ($p = 0.011$) and controls ($p = 0.002$).

All controls demonstrated a central flow jet except one with mild eccentricity. In contrast, none of the patients with stented, stentless or mechanical prosthesis showed a central flow jet. Stented bioprostheses exhibited the most prominent eccentricity among all AVR types with the majority being graded as 'marked' ($p = 0.024$ vs. stentless; $p = 0.001$ vs.

mechanical; $p < 0.001$ vs. autografts; $p < 0.001$ vs. controls). In stentless bioprostheses, eccentric flow was mild in 4 of 8 subjects, and marked in 4. The mean eccentricity score was larger compared to autografts ($p = 0.011$) and controls ($p < 0.001$). In both bioprosthetic types, the eccentric jet was exclusively directed to the right anterior aortic wall. In mechanical prostheses, the majority had mild eccentricity with only 2 of 9 subjects showing marked eccentricity ($p < 0.001$ vs. controls). The jet direction was either to the right anterior side ($n = 6$), or to the opposite left side ($n = 3$). The autograft group was the only type of AVR, which resulted in central flow in 3 of 7 subjects, while the remaining showed mild eccentricities towards the right anterior. Based on the eccentricity score, the autograft group differed from all AVR types ($p = 0.011$ vs. stentless; $p < 0.001$ vs. stented; $p = 0.024$ vs. mechanical), while no significant difference was found compared to controls ($p = 0.056$).

### 3.3. Segmental wall shear stress distribution in the ascending aorta

The segmental distribution of $WSS_{peak}$ along the aortic circumference for each group is illustrated in Fig. 5. Significant group-to-group differences became evident in the left posterior portion of the aortic circumference on the sinotubular level (segments 7, 8, and 9), in the right anterior portion in the mid-ascending aorta (segments 2, 3, and 4) as well as in the right posterior portion in the distal ascending aorta (segments 5 and 7). Table 2 summarizes all the significant $WSS_{peak}$ group-to-group differences. The complete collection of all corresponding results is available in the supplementary material (Tables S1 and S2). On the sinotubular level in the left posterior region, autografts exhibited significantly lower segmental $WSS_{peak}$ results compared to mechanical prostheses and controls. Stented bioprostheses showed lower $WSS_{peak}$ values than mechanical prostheses and controls. In the mid-ascending aorta along the right anterior portion of the aortic wall, stented and stentless bioprostheses showed a marked increase of $WSS_{peak}$ with significant difference to controls and autografts. In the distal ascending aorta along the right posterior aortic portion, stented bioprostheses, autografts and mechanical prostheses exhibited lower $WSS_{peak}$ values than controls.

## 4. Discussion

The understanding of the interaction of AVR and aortic remodeling is important to select the best therapeutic approach for the individual patient. With 4D-flow CMR, we applied a novel technique to acquire information about the flow characteristics in proximity to a replaced aortic valve. This pilot study revealed that all types of AVR were associated with a change in ascending aortic flow characteristics compared to native aortic valves. The blood flow pattern furthermore seemed to differ between various AVR types.

In *autografts*, flow helicity and vorticity widely resembled the observations in healthy controls, with no patients exhibiting marked flow eccentricity. The explanation that both types do not completely agree even though all subjects carry ‘native’ valves may be seen in differences between the pulmonary and the aortic valve morphology [17]. The autograft group showed significantly depressed segmental $WSS_{peak}$ values compared to controls along the circumference of the aortic wall and thus supports recent findings from 2D MRI reporting lower ascending aortic shear rates in autograft patients as compared to controls

[18]. One possible explanation for this difference may be the larger aortic size in the autograft group compared to the controls both in the present study and in the cited 2D MRI study. *Stented bioprostheses* showed considerable differences from the other AVR types and controls. Both vortex and helix scores were significantly elevated. The majority exhibited a markedly eccentric flow jet in the direction of the right anterior portion of the aortic wall. The segmental $WSS_{peak}$ was eccentric along the circumference of the aortic wall with maximum values in the same region where the jet impinged on the aortic wall. Recent studies reported an association between blood flow eccentricity and aortic growth rate in patients with bicuspid aortic valve disease [19]. Furthermore, high WSS was reported to be a hemodynamic condition that predisposes the vessel wall to aneurysm formation [20,21]. Hence, the pattern after AVR with a stented bioprostheses may be an influencing factor for postoperative aortic remodeling. *Stentless bioprostheses* aim to provide superior hemodynamics over stented devices as no stent material impedes blood flow. The present data demonstrated that stentless prostheses were associated with lower vorticity and helicity in the ascending aorta. The mean orifice area in the stentless group was larger than in the stented group, which may have been an influencing factor. Even though the flow eccentricity was less distinct than in stented bioprostheses, all stentless prostheses exhibited a mild or marked eccentric flow jet instead of the central flow seen in healthy controls. The jet was directed to the right anterior aortic wall. Again, segmental $WSS_{peak}$ was elevated at the right anterior portion of the aortic wall and resembled the pattern observed with the stented bioprostheses. This finding is in agreement with previous experimental animal models that reported no difference between stented and stentless valves regarding the formation of turbulence [22]. Whether the biological cusp material impacts the blood flow is hardly determinable due to the small subgroups. Bovine bioprostheses have been reported to be associated with superior hemodynamic results. This aspect requires further investigation in larger samples. *Mechanical prostheses showed* the highest segmental $WSS_{peak}$ results on the sinotubular level with significant difference compared to stented bioprostheses and healthy controls. In addition, mechanical prostheses were associated with the most distinct vortical flow profile in the ascending aorta. These findings may reflect the hemodynamic consequences caused by the rigid opening and closing mechanism and the asymmetric orifices [23]. Interestingly, the mechanical group was the only group that included cases with jet directions oriented to the left side of the aortic wall compared to the predominant pattern exhibiting a right anterior jet. We speculate that the jet direction depends on the orientation of the implanted prosthesis [23]: Based on orientation of the prosthesis in relation to the interventricular septum in a short axis slice, we defined prostheses with the leaflets aligned with the interventricular septum (type 1), and prostheses transverse to the interventricular septum (type 2). All subjects, who exhibited a jet direction to the right-anterior aortic wall had type 2 orientations, while all subjects with jet direction to the left had type 1.

The present data furthermore demonstrated that bioprostheses produced markedly eccentric flow more often than mechanical valves. The explanation may be differences in the opening mechanism and in the sensibility to co-factors like the angle between the open cusp and the annular plane [23,24]. We speculate that the orifice of the mechanical prosthesis might act like a central channel stabilizing the blood flow close to the aortic center, while the blood

flow of bioprostheses experiences a stronger deviation. This hypothesis might also be the reason, why the WSS results showed an asymmetric pattern for bioprostheses and a quite homogenous distribution for mechanical prostheses.

### 4.1. Study limitations

i) The study sample is small and there is relevant inter-group heterogeneity regarding factors with potential influence on aortic hemodynamics. For instance, the dependency of blood flow characteristics from age and aortic dimensions as well as the opening angle between the aortic cusp and the annular plane has previously been reported [16,25,24]. In addition, medical treatment with anticoagulants influences blood viscosity, which then may impact WSS. ii) The study does not provide a longitudinal observation to analyze the interaction of ascending aortic flow characteristics and aortic remodeling. In order to define a causal effect of ascending aortic flow characteristics on the aortic remodeling, prospective follow-up studies with samples large enough to correct for confounding variables are needed. iii) The semiquantification of vorticity and helicity is limited by its subjective visual nature and by focusing on the direction of the particles, while the amount of deviating particles remains unconsidered. Further development of post-processing may provide more objective tools to characterize flow patterns in the future [26]. iv) Assessment of WSS distribution using 4D-flow MR is limited by spatial and temporal resolution and moderate signal-to-noise ratio at 1.5 T [27]. True WSS results may be higher than the WSS results obtained by CMR [13]. In addition, suboptimal velocity encoding, turbulence and disturbance of the magnetic field by the prosthesis might have negatively impacted the accuracy of the results. Thus, imaging settings were chosen to find reasonable compromises between scan duration, resolution, SNR, and VENC, and measurement planes were selected to be distant from the prosthesis itself. The method appears appropriate to assess at least the relative differences between individual WSS patterns, if the procedure of WSS estimation is consistent between study populations as in our cohorts. v) The rate of patient exclusion from the study was high with the reason for exclusion being in most cases clinical–technical in nature. To realize larger patient studies or promote clinical application, further developments for faster and more robust image acquisition are required.

## 5. Conclusion

In conclusion, this pilot study showed that the flow characteristics in the ascending aorta are influenced by any AVR. These data indicate the potential of 4D-flow MRI to obtain new insights into ascending aortic hemodynamics adjacent to various types of AVR. The application of this technique in larger AVR samples with matched controls and with longitudinal follow-up studies is needed to analyze any relation between ascending aortic flow characteristics and aortic remodeling.

## Supplementary Material

Refer to Web version on PubMed Central for supplementary material.

## Acknowledgments

We thank our technicians Kerstin Kretschel, Evelyn Polzin and Denise Kleindienst for performing the CMR scans, and Dr. Carsten Schwenke (scossis, Berlin, Germany) for supporting the statistical analysis.

## Appendix A. Supplementary data

Supplementary data to this article can be found online at http://dx.doi.org/10.1016/j.ijcard.2013.11.034

## References

1. Gaudino M, Anselmi A, Morelli M, et al. Aortic expansion rate in patients with dilated post-stenotic ascending aorta submitted only to aortic valve replacement long-term follow-up. J Am Coll Cardiol. 2011; 58:581–4. [PubMed: 21798419]
2. Botzenhardt F, Hoffmann E, Kemkes BM, Gansera B. Determinants of ascending aortic dimensions after aortic valve replacement with a stented bioprosthesis. J Heart Valve Dis. 2007; 16:19–26. [PubMed: 17315379]
3. Cozijnsen L, Braam RL, Waalewijn RA, et al. What is new in dilatation of the ascending aorta? Review of current literature and practical advice for the cardiologist. Circulation. 2011; 123:924–8. [PubMed: 21357847]
4. Malek AM, Alper SL, Izumo S. Hemodynamic shear stress and its role in atherosclerosis. J Am Med Assoc. 1999; 282:2035–42.
5. Cecchi E, Giglioli C, Valente S, et al. Role of hemodynamic shear stress in cardiovascular disease. Atherosclerosis. 2011; 214:249–56. [PubMed: 20970139]
6. Frydrychowicz A, Stalder AF, Russe MF, et al. Three-dimensional analysis of segmental wall shear stress in the aorta by flow-sensitive four-dimensional-MRI. J Magn Reson Imaging. 2009; 30:77–84. [PubMed: 19557849]
7. Hope MD, Hope TA, Crook SE, et al. 4D flow CMR in assessment of valve-related ascending aortic disease. JACC Cardiovasc Imaging. 2011; 4:781–7. [PubMed: 21757170]
8. Barker AJ, Markl M, Burk J, et al. Bicuspid aortic valve is associated with altered wall shear stress in the ascending aorta. Circ Cardiovasc Imaging. 2012; 5:457–66. [PubMed: 22730420]
9. von Knobelsdorff-Brenkenhoff F, Dieringer MA, Greiser A, Schulz-Menger J. In vitro assessment of heart valve bioprostheses by cardiovascular magnetic resonance: four-dimensional mapping of flow patterns and orifice area planimetry. Eur J Cardiothorac Surg. 2011; 40:736–42. [PubMed: 21342775]
10. von Knobelsdorff-Brenkenhoff F, Rudolph A, Wassmuth R, et al. Feasibility of cardiovascular magnetic resonance to assess the orifice area of aortic bioprostheses. Circ Cardiovasc Imaging. 2009; 2:397–404. [PubMed: 19808628]
11. von Knobelsdorff-Brenkenhoff F, Rudolph A, Wassmuth R, Abdel-Aty H, Schulz-Menger J. Aortic dilatation in patients with prosthetic aortic valve: comparison of MRI and echocardiography. J Heart Valve Dis. 2010; 19:349–56. [PubMed: 20583398]
12. Hiratzka LF, Bakris GL, Beckman JA, et al. 2010 ACCF/AHA/AATS/ACR/ASA/SCA/SCAI/SIR/STS/SVM guidelines for the diagnosis and management of patients with thoracic aortic disease. A report of the American College of Cardiology Foundation/American Heart Association Task Force on Practice Guidelines, American Association for Thoracic Surgery, American College of Radiology, American Stroke Association, Society of Cardiovascular Anesthesiologists, Society for Cardiovascular Angiography and Interventions, Society of Interventional Radiology, Society of Thoracic Surgeons, and Society for Vascular Medicine. J Am Coll Cardiol. 2010; 55:e27–129. [PubMed: 20359588]
13. Stalder AF, Russe MF, Frydrychowicz A, Bock J, Hennig J, Markl M. Quantitative 2D and 3D phase contrast MRI: optimized analysis of blood flow and vessel wall parameters. Magn Reson Med. 2008; 60:1218–31. [PubMed: 18956416]

14. Markl M, Wallis W, Harloff A. Reproducibility of flow and wall shear stress analysis using flow-sensitive four-dimensional MRI. J Magn Reson Imaging. 2011; 33:988–94. [PubMed: 21448968]
15. Zoghbi WA, Chambers JB, Dumesnil JG, et al. Recommendations for evaluation of prosthetic valves with echocardiography and doppler ultrasound: a report From the American Society of Echocardiography's Guidelines and Standards Committee and the Task Force on Prosthetic Valves, developed in conjunction with the American College of Cardiology Cardiovascular Imaging Committee, Cardiac Imaging Committee of the American Heart Association, the European Association of Echocardiography, a registered branch of the European Society of Cardiology, the Japanese Society of Echocardiography and the Canadian Society of Echocardiography, endorsed by the American College of Cardiology Foundation, American Heart Association, European Association of Echocardiography, a registered branch of the European Society of Cardiology, the Japanese Society of Echocardiography, and Canadian Society of Echocardiography. J Am Soc Echocardiogr. 2009; 22:975–1014. [quiz 1082–1014]. [PubMed: 19733789]
16. Geiger J, Markl M, Herzer L, et al. Aortic flow patterns in patients with Marfan syndrome assessed by flow-sensitive four-dimensional MRI. J Magn Reson Imaging. 2012; 35:594–600. [PubMed: 22095635]
17. Gross L, Kugel MA. Topographic anatomy and histology of the valves in the human heart. Am J Pathol. 1931; 7:445–74 [447]. [PubMed: 19969978]
18. Torii R, El-Hamamsy I, Donya M, et al. Integrated morphologic and functional assessment of the aortic root after different tissue valve root replacement procedures. J Thorac Cardiovasc Surg. 2012; 143:1422–8. [PubMed: 22361248]
19. Hope MD, Wrenn J, Sigovan M, Foster E, Tseng EE, Saloner D. Imaging biomarkers of aortic disease: increased growth rates with eccentric systolic flow. J Am Coll Cardiol. 2012; 60:356–7. [PubMed: 22813616]
20. Meng H, Wang Z, Hoi Y, et al. Complex hemodynamics at the apex of an arterial bifurcation induces vascular remodeling resembling cerebral aneurysm initiation. Stroke. 2007; 38:1924–31. [PubMed: 17495215]
21. Dolan JM, Meng H, Singh S, Paluch R, Kolega J. High fluid shear stress and spatial shear stress gradients affect endothelial proliferation, survival, and alignment. Ann Biomed Eng. 2011; 39:1620–31. [PubMed: 21312062]
22. Funder JA. Current status on stentless aortic bioprosthesis: a clinical and experimental perspective. Eur J Cardiothorac Surg. 2012; 41:790–9. [PubMed: 22219434]
23. Yoganathan AP, He Z, Casey Jones S. Fluid mechanics of heart valves. Annu Rev Biomed Eng. 2004; 6:331–62. [PubMed: 15255773]
24. Della Corte A, Bancone C, Conti CA, et al. Restricted cusp motion in right-left type of bicuspid aortic valves: a new risk marker for aortopathy. J Thorac Cardiovasc Surg. 2012; 144:360–9 [369 e361]. [PubMed: 22050982]
25. Bogren HG, Buonocore MH, Valente RJ. Four-dimensional magnetic resonance velocity mapping of blood flow patterns in the aorta in patients with atherosclerotic coronary artery disease compared to age-matched normal subjects. J Magn Reson Imaging. 2004; 19:417–27. [PubMed: 15065165]
26. Lorenz, R.; Bock, J.; Barker, AJ., et al. 4D flow magnetic resonance imaging in bicuspid aortic valve disease demonstrates altered distribution of aortic blood flow helicity. Magn Reson Med. 2013. http://dx.doi.org/10.1002/mrm.24802
27. Strecker C, Harloff A, Wallis W, Markl M. Flow-sensitive 4D MRI of the thoracic aorta: comparison of image quality, quantitative flow, and wall parameters at 1.5 T and 3 T. J Magn Reson Imaging. 2012; 36:1097–103. [PubMed: 22745007]

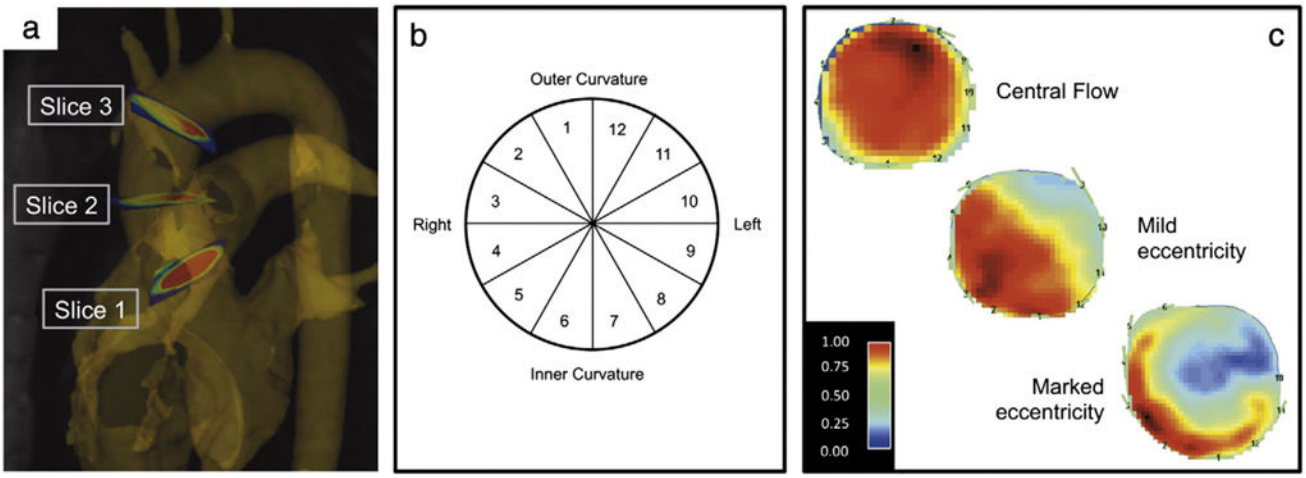


**Fig. 1.**

Methodological schematic: a) position of the analysis planes in the ascending aorta on the level of the sinotubular junction (S1), mid-ascending (S2) and distal ascending aorta (S3). b) Cross-section of the ascending aorta that describes the distribution of the segments along the aortic wall circumference. c) Peak systolic flow map at the level of the mid-ascending aorta demonstrating central systolic flow, mild and markedly eccentric systolic flow.

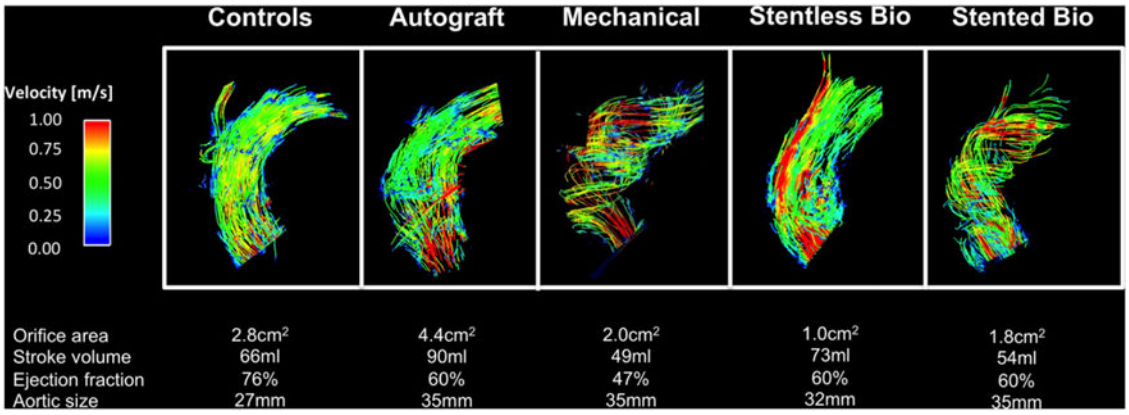


**Fig. 2.**

Visualization of the blood flow in the ascending aorta using particle traces during peak systole for each type of AVR. Relevant anatomic and functional data are given for the individuals below.

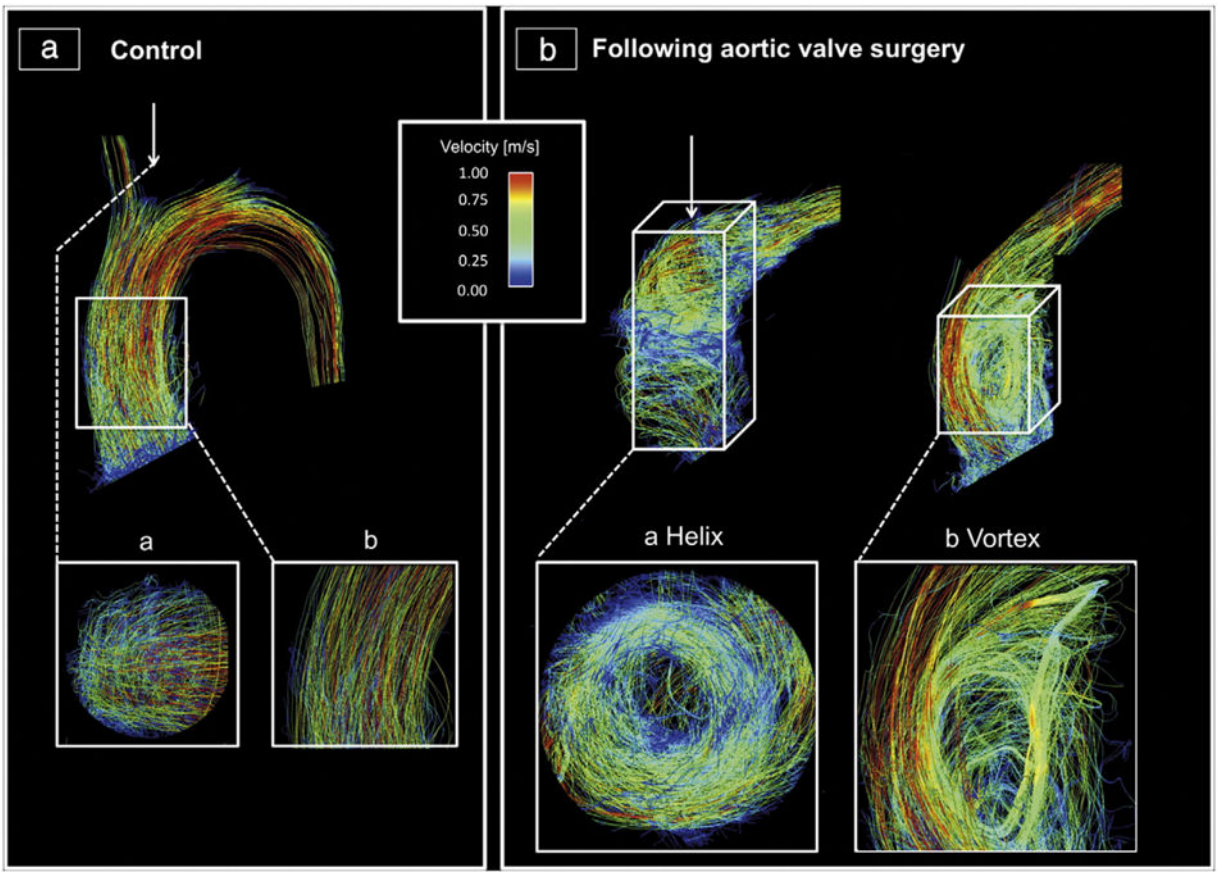


**Fig. 3.**

Visualization of the blood flow in the ascending aortic using streamlines during peak systole: A: Healthy volunteer with cohesive systolic streamlines with mild helical (a) and no vortical (b) flow. B: Two exemplary cases with AVR, who exhibited helical (a) and vortical (b) flow each graded as severe. a) A mechanical prosthesis (St. Jude Medical 21); b) a stented bioprostheses (Medtronic Freestyle 25). The helical flow is shown in a transverse cut plane, whereas the vortex is shown in a sagittal cut plane.

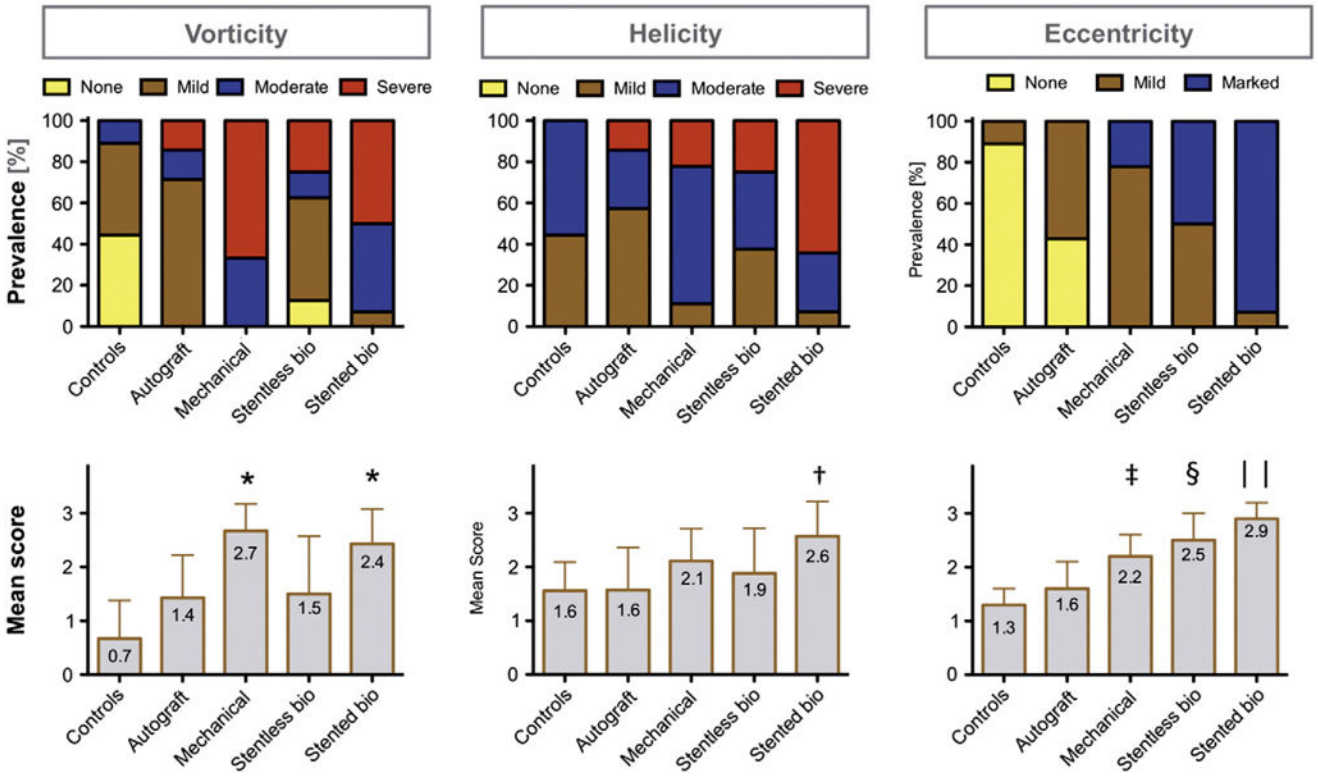


**Fig. 4.**

Evaluation of vorticity, helicity and eccentricity of blood flow: The upper row shows the frequency of each score for the various AVR groups and controls. The lower row depicts the mean ± SD scoring results (*$p < 0.05$ vs. stentless, autografts and controls; $^{\dagger}p < 0.05$ vs. stentless, autografts and controls; $^{\ddagger}p < 0.05$ vs. controls; $^{\$}p < 0.05$ vs. stented, autografts, controls; $^{\|}p < 0.05$ vs. stentless, mechanical, autografts and controls).

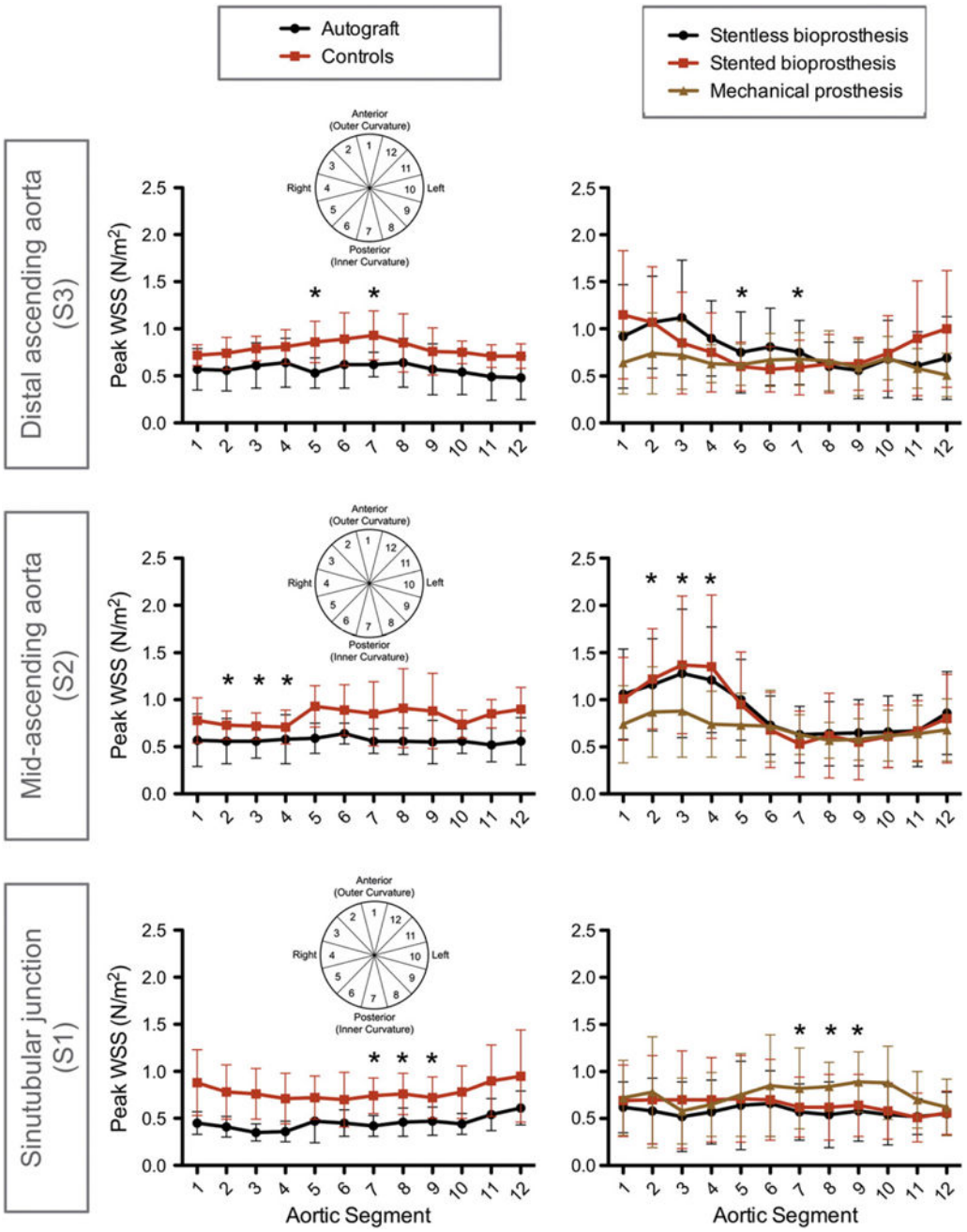


**Fig. 5.**

Segmental distribution of $WSS_{peak}$ along the circumference of the aortic wall for aortic levels S1–S3 for all groups of AVR and the controls. The aortic segments 1–12 correspond to the anatomic regions as outlined in Fig. 1 (which is additionally displayed in miniature within the graphs here). Roughly, “3–5” = right, “9–11” = left, “12–2” = outer curvature, “6–8” = inner curvature. Asterisk indicates the presence of any significant inter-group difference at the given aortic location and refers to the statistical results of Table 2.

**Table 1**

Characteristics of the study participants.

| Parameter | Controls | Autograft | Mechanical | Stentless bio | Stented bio | *p* |
|---|---|---|---|---|---|---|
| *n* | 9 | 7 | 9 | 8 | 14 | – |
| Sex (females/males) | 1/8 | 2/5 | 0/9 | 2/6 | 4/10 | – |
| Age (years) | 55 ± 16 | 47 ± 17 | 61 ± 11 | 62 ± 20 | 77 ± 4 | <0.001* |
| Native valvular lesion | – | Stenosis (*n* = 3), regurgitation (*n* = 1), mixed (*n* = 3) | Stenosis (*n* = 3), regurgitation (*n* = 5), mixed (*n* = 1) | Stenosis (*n* = 5), regurgitation (*n* = 3) | Stenosis (*n* = 7), regurgitation (*n* = 2), mixed (*n* = 5) | – |
| Time since valve surgery [years] | – | 6.0 ± 4.2 | 7.9 ± 3.6 | 2.7 ± 4.8 | 3.6 ± 2.6 | 0.014* |
| Labeled valve size | – | – | 24.3 ± 2.5 | 26.0 ± 1.5 | 23.6 ± 2.0 | 0.029* |
| Orifice area [$cm^2$] | 4.0 ± 0.8 | 4.6 ± 0.9 | 1.8 ± 0.5 | 2.0 ± 0.5 | 1.5 ± 0.4 | <0.001* |
| Orifice area index [$cm^2/m^2$] | 2.0 ± 0.4 | 2.3 ± 0.4 | 0.9 ± 0.2 | 1.1 ± 0.3 | 0.8 ± 0.2 | <0.001* |
| Prosthetic types | – | – | Only bileaflet valves. Levibio ATS (*n* = 1), Sorin Carbomedics (*n* = 1), Medtronic Advantage (*n* = 1), St. Jude Regent (*n* = 6) | Porcine: Vascutek Elan (*n* = 1), Shelhigh (*n* = 3); St. Jude Toronto (*n* = 1); bovine: Sorin Freedom Solo (*n* = 2); Medtronic Freestyle (*n* = 1) | Porcine: Medtronic Hancock (*n* = 6), Labcore (*n* = 1); bovine: Edwards Perimount (*n* = 3), Sorin Mitroflow (*n* = 2), unknown (*n* = 2) | – |
| LV end diastolic volume [ml] | 140 ± 41 | 176 ± 34 | 186 ± 98 | 165 ± 64 | 147 ± 58 | 0.459 |
| LV stroke volume [ml] | 92 ± 28 | 98 ± 22 | 76 ± 51 | 98 ± 40 | 84 ± 31 | 0.585 |
| LV ejection fraction [%] | 66 ± 6 | 57 ± 13 | 50 ± 14 | 60 ± 10 | 59 ± 11 | 0.049* |
| Aortic diameter [mm] | 31 ± 5 | 37 ± 4 | 40 ± 8 | 37 ± 7 | 38 ± 4 | 0.009* |

Results are given as frequencies or as mean ± SD. The *p*-value relates to the Kruskal–Wallis multiple group comparison. Further inter-study relations are outlined in the text.

## Table 2

Comparison of the segmental $WSS_{peak}$ between the groups on the different aortic levels (S1–S3).

| | Pairwise comparison | Aortic segment | $WSS_{peak}$ [$N/m^2$] | *p* |
|---|---|---|---|---|
| Sinotubular junction (S1) | Autografts vs. mechanical | 7 | 0.4 ± 0.1 vs. 0.8 ± 0.4 | 0.039 |
| | | 8 | 0.5 ± 0.2 vs. 0.8 ± 0.3 | 0.003 |
| | | 9 | 0.5 ± 0.2 vs. 0.9 ± 0.3 | 0.004 |
| | Autografts vs. controls | 8 | 0.5 ± 0.2 vs. 0.8 ± 0.2 | 0.010 |
| | | 9 | 0.5 ± 0.2 vs. 0.7 ± 0.2 | 0.017 |
| | Mechanical vs. Stented bio | 8 | 0.8 ± 0.3 vs. 0.6 ± 0.4 | 0.010 |
| | | 9 | 0.9 ± 0.3 vs. 0.6 ± 0.3 | 0.038 |
| | Stented bio vs. controls | 8 | 0.6 ± 0.4 vs. 0.8 ± 0.2 | 0.027 |
| Mid-ascending aorta (S2) | Stented bio vs. controls | 2 | 1.2 ± 0.5 vs. 0.7 ± 0.2 | 0.004 |
| | | 3 | 1.4 ± 0.7 vs. 0.7 ± 0.1 | 0.017 |
| | Stented bio vs. autografts | 2 | 1.2 ± 0.5 vs. 0.6 ± 0.2 | 0.004 |
| | | 3 | 1.4 ± 0.7 vs. 0.6 ± 0.2 | 0.005 |
| | | 4 | 1.4 ± 0.8 vs. 0.6 ± 0.3 | 0.030 |
| | Stentless bio vs. autografts | 2 | 1.2 ± 0.5 vs. 0.6 ± 0.2 | 0.008 |
| | | 3 | 1.3 ± 0.7 vs. 0.6 ± 0.2 | 0.008 |
| | | 4 | 1.2 ± 0.6 vs. 0.6 ± 0.3 | 0.028 |
| | Stentless bio vs. controls | 3 | 1.3 ± 0.7 vs. 0.7 ± 0.1 | 0.027 |
| Distal ascending aorta (S3) | Stented bio vs. controls | 5 | 0.6 ± 0.3 vs. 0.9 ± 0.2 | 0.006 |
| | | 7 | 0.6 ± 0.3 vs. 0.9 ± 0.3 | 0.003 |
| | Autografts vs. controls | 5 | 0.5 ± 0.2 vs. 0.9 ± 0.2 | 0.004 |
| | | 7 | 0.6 ± 0.1 vs. 0.9 ± 0.3 | 0.007 |
| | Mechanical vs. controls | 5 | 0.6 ± 0.2 vs. 0.9 ± 0.2 | 0.019 |

The table only summarizes the comparisons that reached significance. The full set of results is available as supplemental material.